Natural Hazards
and Earth System
Sciences

The importance of entrainment and bulking on debris flow runout modeling: examples from the Swiss Alps

F. Frank[1], B. W. McArdell[1], C. Huggel[2], and A. Vieli[2]

[1]Swiss Federal Institute for Forest, Snow and Landscape Research WSL, Birmensdorf, Switzerland
[2]Department of Geography, University of Zurich-Irchel, Zurich, Switzerland

Correspondence to: B. W. McArdell (brian.mcardell@wsl.ch)

Abstract. This study describes an investigation of channel-bed entrainment of sediment by debris flows. An entrainment model, developed using field data from debris flows at the Illgraben catchment, Switzerland, was incorporated into the existing RAMMS debris-flow model, which solves the 2-D shallow-water equations for granular flows. In the entrainment model, an empirical relationship between maximum shear stress and measured erosion is used to determine the maximum potential erosion depth. Additionally, the average rate of erosion, measured at the same field site, is used to constrain the erosion rate. The model predicts plausible erosion values in comparison with field data from highly erosive debris flow events at the Spreitgraben torrent channel, Switzerland in 2010, without any adjustment to the coefficients in the entrainment model. We find that by including bulking due to entrainment (e.g., by channel erosion) in runout models a more realistic flow pattern is produced than in simulations where entrainment is not included. In detail, simulations without entrainment show more lateral outflow from the channel where it has not been observed in the field. Therefore the entrainment model may be especially useful for practical applications such as hazard analysis and mapping, as well as scientific case studies of erosive debris flows.

1 Introduction

Debris flows in mountain areas are one of the most important landscape forming processes in high alpine catchments. Numerous debris fans as well as larger and lower-angled alluvial fans were constructed at least partly by debris flows, mostly after the deglaciation at the beginning of Holocene (Kober et al., 2012). In recent decades, previously stable sediment deposits or rock walls became destabilized in the Swiss Alps (Huggel et al., 2011; Tobler et al., 2014). As a consequence, relatively large debris flow events occurred. The problem has become worse due to increased sediment input connected to intense rainfall activity (e.g., Tobler et al., 2014) or in some cases snowmelt activity in early summer (e.g., Graf et al., 2013) which can readily mobilize the debris. The recent large debris flows are unusual in that they have caused unprecedented amounts of erosion on the debris fans or alluvial fans, thereby increasing awareness of the importance of debris-flow entrainment, especially for practical applications such as runout analysis and hazard mapping (e.g., Rickenmann and Zimmermann, 1993; Kienholz et al., 2010).

Recent debris flow research mainly focused on the bulk properties and the physical behavior of the debris flow process itself (e.g., Iverson, 1997; McArdell et al., 2007; Jakob and Hungr, 2005). Physically based numerical models were developed to investigate runout distance and inundation patterns as well as flow heights and flow velocities (Crosta et al., 2003; D'Ambrosio et al., 2003; Medina et al., 2008; Hungr and McDougall, 2009; Christen et al., 2012). Only recently have researchers focused on better understanding the process by which debris flows entrain sediment from the bed of a torrent channel as part of the erosion process (e.g., Hungr et al., 2005; Mangeney et al., 2007; Berger et al., 2011; Iverson et al., 2011; McCoy et al., 2010, 2012, 2013).

Runout models are an increasingly applied tool to reconstruct previous events and simulate scenarios of debris flow events for research and practical application. One challenge with the application of runout models for hazard analysis is that the initial volume of the debris flow entering a reach,

e.g., at the upstream end of a modeling project site, is often substantially smaller than the volume of the debris flow leaving the reach due to entrainment of sediment from the channel bed along the channel.

In current debris flow runout models without entrainment, to achieve the design volume for the lowermost object of interest along a torrent channel (e.g., a village on the lower fan), it is necessary to start the model with all of the debris flow volume at the upstream end. This may result in an over-prediction of debris flow discharge and flow depth at the upstream end of the channel, especially if channel erosion occurs. Overflow occurs in places where the modeled discharge is larger than the channel capacity. The loss of a considerable portion of modeled material due to lateral overflow and overbank deposition can even lead to an under-prediction of the runout distance. On the contrary, when implementing the observed initial volume at the upstream end, a runout model without entrainment tends to under-predict the runout patterns. Both approaches could therefore lead to unrealistic hazard assessments. A runout model including entrainment can potentially improve the quality of the prediction of observed flow patterns by improving the accuracy of the prediction of flow depth and discharge along the flow path due to the entrainment of sediment and the increase in volume and peak discharge of a debris flow.

Debris flow entrainment modeling has been introduced into runout models using algorithms considering the properties of the debris flow (Crosta et al., 2003; D'Ambrosio et al., 2003; Medina et al., 2008). Another approach relies on user-specified erosion layer properties (Beguería et al., 2009; Hungr and McDougall, 2009; Hussin et al., 2012) where the user predefines the volume or depth of eroded sediment. An example for this model type was implemented by Hussin et al. (2012) within the RAMMS 2-D debris flow runout model (Christen et al., 2012). Hussin et al. (2012) used a predefined entrainment method including one or more erosion layers with an absolute thickness specified by the model user wherein an erosion layer is instantaneously eroded when a user-specified critical shear stress is exceeded. This approach is based on the work of Sovilla et al. (2006) for describing the entrainment of snow by avalanches. However, in these modeling approaches, the user often must pre-specify the thickness of the erodible layer.

Field observations of the entrainment of sediment from torrent channel beds are rather rare. Rickenmann et al. (2003) studied debris-flow erosion in field and laboratory experiments. They concluded that the fragmentation of material from a matrix (gravel bed or bedrock) depends on the exposure of the particle to the basal forces acting on the matrix, and furthermore that the removal of sediment increases with increasing water content. To assess the timing and the absolute erosion depth caused by natural debris flows at the Illgraben channel, Berger et al. (2010a, 2011) installed a novel channel bed erosion sensor based on the concept of an electrical resistance chain. McCoy et al. (2013) recently studied

basal forces generated by erosive debris flows in Chalk Cliff catchment, Denver, Colorado USA, using a similar type of instrumentation consisting of erosion sensors similar to those in the Illgraben as well as erosion bolts in bedrock and a small force plate. They concluded that debris flows in the field show much broader distributions of basal force than in the laboratory, which they attributed to wider grain size distributions observed in the field. Laboratory results are, in any case, difficult to apply for investigating debris-flow erosion due to problems arising when scaling small-scale laboratory results to the field (e.g., Iverson and Denlinger, 2001; Rickenmann et al., 2003; Reid et al., 2011; McCoy et al., 2013). Therefore we focus on a field-data-based entrainment approach in our study.

The goal of this paper is to demonstrate the importance of debris-flow entrainment for runout modeling, which could be used for hazard assessment. To achieve this goal, we developed and implemented a field-data-based empirical erosion model within a debris-flow runout model and use it as a tool to assess the potential importance of debris-flow entrainment. Potential applications in the future will include both post-event analysis and hazard analysis for future events.

2 The entrainment model development site: Illgraben catchment, Switzerland

The catchment of the Illgraben torrent is located in southern Switzerland, in Canton Valais (Fig. 1a) and has an area of overall 10.9 km² (Fig. 1b). The Vanoischi subcatchment (Fig. 1b) produces several debris flows every year and covers only 4.6 km². The geology of the sediment-delivering north-facing wall below the Illhorn mountain (2.717 m a.s.l.) is comprised mainly of banded quartzite, while the opposite wall consists of dolomites and dolomite breccias which form massive cliffs (Gabus et al., 2008). The north facing side of the catchment is quite heavily exposed to surface erosion processes and frequently delivers sediment into the debris flow initiation zones (Bennet et al., 2012, 2013).

The main debris flow activity at Illgraben is from May through October and is mostly due to convective rainstorms. The resulting runoff mobilizes sediment deposits in steep bedrock channels ($> 30°$) (Berger et al., 2010b). Because of its high degree of debris-flow activity, this catchment became one of the most studied debris flow sites in the Alps. During the last decade, studies focused on various aspects of the debris flow process addressing the flow process itself (Hürlimann et al., 2003; McArdell et al., 2007), developing a reliable warning system for debris flows based on flow detection (Badoux et al., 2009), studying sediment transfer (Berger et al., 2010b; Bennet et al., 2012, 2013) and the erosion process (Berger et al., 2010a, b, 2011; Schürch et al., 2011a, b; Bennet et al., 2014). Today, the channel is equipped with several measurement installations which allow estimation of typical flow parameters such as front velocity and flow depth. Other
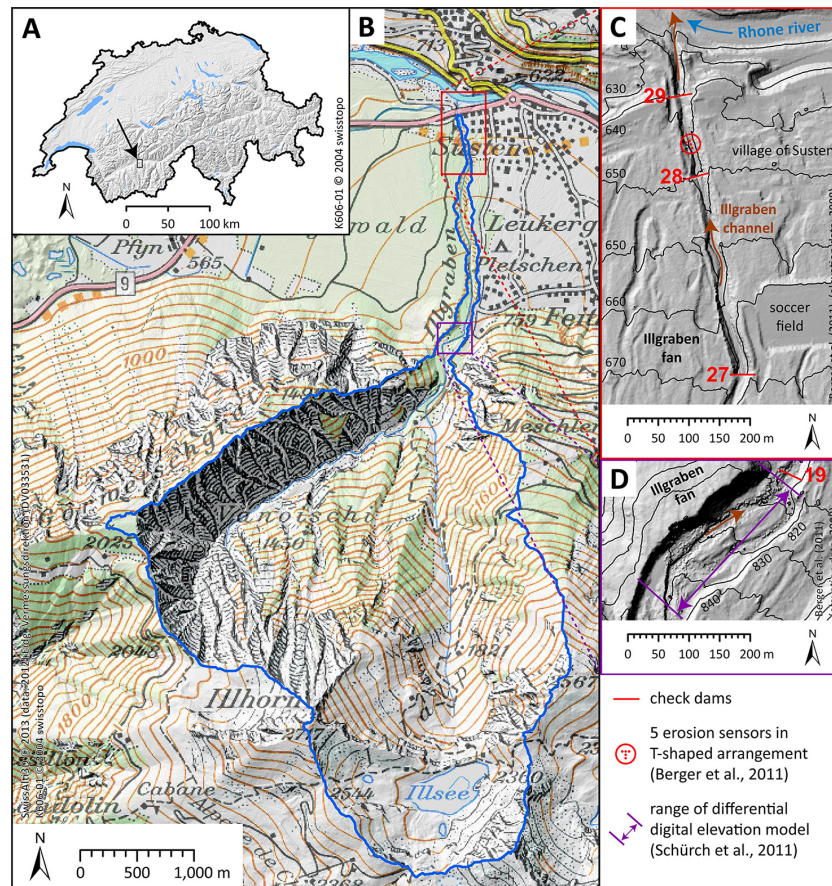
Figure 1. (a) The Illgraben catchment in southern Switzerland. **(b)** Locations of the instrumentation site and data available for the erosion analysis at the Illgraben catchment. **(c)** On the lower fan of Illgraben, the location of the erosion sensors (Berger et al., 2011) and main instrumentation site (McArdell et al., 2007) on check dam 29 is shown. **(d)** The channel reach covered by the terrestrial laser scanning-based elevation-change analysis (Schürch et al., 2011b) is located on the upper fan below the fan apex.

debris flow properties are measured using force plates on the channel bed and on a lateral wall to determine basal and lateral stresses as well as bulk density (McArdell et al., 2007; Berger et al., 2011; Schürch et al., 2011b).

3 The entrainment model application site: Spreitgraben, Switzerland

The catchment of the Spreitgraben torrent is located in Central Switzerland, near the village of Guttannen at the north side of the Grimselpass in Canton Bern (Fig. 2a). The catchment area is about 4.25 km². Foliated gneisses of the Aare massif consisting of crystalline rock dominate the geology. The steep rock wall below the Ritzlihorn (3.263 m a.s.l.) is exposed to the northeast and has steep gullies and couloirs across its entire width. Weathering processes cause frequent sediment supply mostly by rockfall and snow avalanches. The largest activity occurs from spring until mid-summer (April to July) (Geotest, 2010). A considerable increase in rockfall frequency has been observed during springtime. Fur-

thermore, permafrost degradation above 2.700 m a.s.l. was suggested to have contributed to the occurrence of a rock avalanche recorded on 17 July 2009 which deposited about 50 000 m³ of fresh sediment (Geotest, 2010) at the Schafegg slope on the Ritzlihorn. Consequently, debris flow initiation within these deposits increased in frequency and led to a destabilization of the ice–firn–debris mixture below the rock wall in 2010 and more intensively in 2011 (Fig. 2b; Geotest, 2012). During the years 2009–2011 a total volume of more than 600 000 m³ of sediment were transported into the Hasli-aare River (Tobler et al., 2014).

For the active year 2010 at Spreitgraben – when the first two highly erosive debris flows occurred – two lidar-based digital terrain models (DTM) are available. They were collected in middle April 2010 and middle of August 2010, and cover the entire active part of the debris flow channel for the debris flow events in 2010 (Table 1).

These 2010 debris flow events extend from the bottom of the Ritzlihorn wall down to the most far-reaching debris depositions in the valley of the Hasliaare River near the village
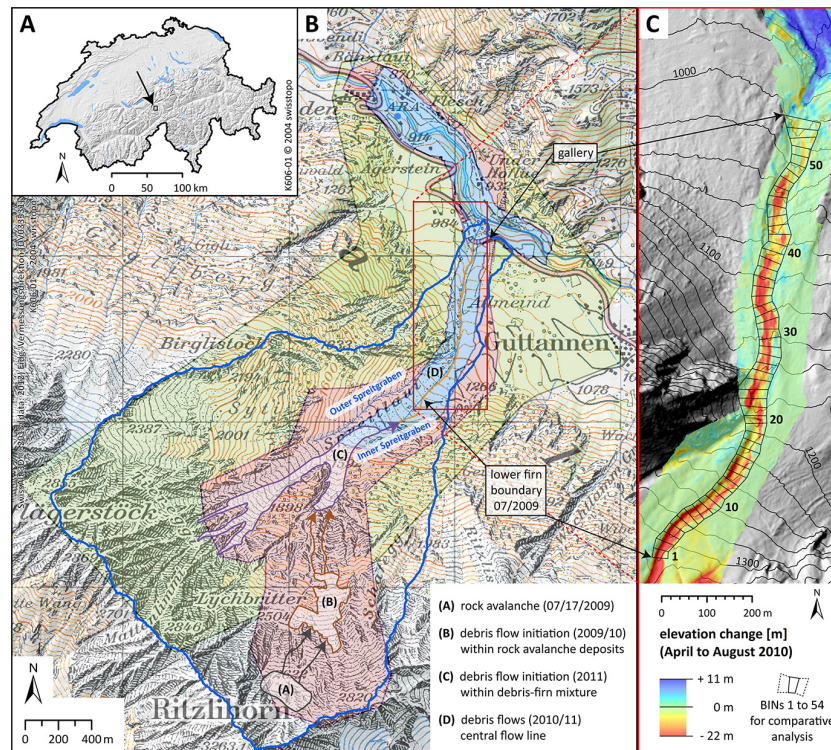
Figure 2. (a) The Spreitgraben catchment in Central Switzerland. **(b)** The processes observed in the catchment **(a)** to **(d)** during the most active years 2009 to 2011 and the coverage of the three available lidar-based digital terrain models DTM (2010 and 2011) for the erosion analysis: 04/2010 (raster cell: 2 m, blue polygon); 08/2010 (raster cell: 1m, red polygon); 10/2011 (raster cell: 1 m, green polygon). **(c)** The elevation change (04/2010 to 08/2010) on the middle and lower fan are compared to erosion modeling results using bins numbered 1 to 54.

Table 1. Data available for the erosion (modeling) analysis for the Spreitgraben (Geotest, 2012). The erosion depth and digital elevation models (DTM) provide the basis for the elevation change data sets.

Data set	Spreitgraben 2010		
debris flow events	07/12/2010 07/16/2010 07/21/2010	07/23/2010	08/12/2010
estimated event volumes [m^3]	$3 \times \approx 10\,000$	$\approx 90\,000$	$\approx 130\,000$
flow height/ discharge data	estimated using videos[1]		
erosion data	field observations[1]		
elevation data available for erosion analysis	lidar-based digital terrain models DTM[2] 04/2010 (cell size = 2 m) and 08/2010 (cell size = 1 m)		

[1] Geotest (2010); [2] cantonal authorities, Bern, Switzerland (2010).

Boden (Fig. 2). For various channel sections, these DTMs allow determination of the elevation changes which occurred during the debris flow season (2010) at the Spreitgraben. The erosion and deposition along the channel is systematically analyzed based on the discretization of the Spreitgraben channel on the fan into 54 bins of similar length (≈ 20 m) along the central flow line. Bins 1 to 54 are located between the former lower firn boundary (1.310 m a.s.l.) of the Inner

Spreitgraben (July 2009) and the gallery of the Grimselpass road just above the confluence (940 m a.s.l.) into the Hasli-aare Valley (Fig. 2c). The erosion observed within the bins is the net bed level change and the erosion volume per bin area [m^3 m^{-2}] yields the net bed level change (m of vertical erosion) within each bin (Sect. 5).

4 Debris-flow entrainment modeling method

The RAMMS debris-flow runout model (rapid mass movement system) was selected for this project because it is already a widely used model for practical (e.g., Scheuner et al., 2011) as well as scientific debris flow applications (e.g., Hussin et al., 2012). However, it would be possible to incorporate the erosion algorithm into other debris flow runout models.

To investigate the importance of debris-flow entrainment on the runout of debris flows, we modified the RAMMS runout model to include a field-data-based algorithm to describe the incorporation of channel-bed sediment into a debris flow. First we describe the governing equations of the runout model, and then we describe the development of the erosion algorithm. The erosion algorithm is empirical and based on field data (Berger et al., 2011; Schürch et al., 2011b), and it describes the potential erosion depth as a function of the basal shear stress produced by the debris flow. Because it is empirical, it has to be applied with caution to other field sites.

Finally, the model is applied and evaluated at the example of two large debris flow events from Spreitgraben, Switzerland.

4.1 Computational debris-flow model RAMMS

The RAMMS debris-flow model uses the 2-D depth-averaged shallow water equations for granular flows in three dimensions given by the coordinates of the topographic surface of the digital elevation model in a Cartesian coordinate system (x, y, z) and at time (t) (Bartelt et al., 1999; Christen et al., 2010). The mass balance equation incorporating the field variables flow height $H(x, y, t)$ and flow velocity $U(x, y, t)$ is given by

$$\dot{Q}(x, y, t) = \partial_t H + \partial_x (HU_x) + \partial_y (HU_y),\tag{1}$$

where $\dot{Q}(x, y, t)$ denotes the mass production source term and U_x and U_y are the depth-averaged velocities in horizontal directions x and y (Christen et al., 2010). The conservation of momentum in two directions x and y is given by the following depth-averaged momentum balance equations:

$$S_{g_x} - S_{f_x} = \partial_t (HU_x) + \partial_x \left(c_x HU_x^2 + g_z k_{a/p} \frac{H^2}{2}\right)\tag{2}$$
$$+ \partial_y (HU_x U_y),$$
$$S_{g_y} - S_{f_y} = \partial_t (HU_y) + \partial_x (HU_x U_y)\tag{3}$$
$$+ \partial_y \left(c_y HU_y^2 + g_z k_{a/p} \frac{H^2}{2}\right),$$

where the earth pressure coefficient $k_{a/p}$ is normally set to 1 when using the standard Voellmy–Salm friction approach, c_x and c_y are topographical coefficients determined from the digital elevation model, S_g represents the effective gravita-

tional acceleration, and S_f the frictional deceleration in directions x and y (Christen et al., 2010). The frictional deceleration S_f of the flow is calculated using the Voellmy friction relation (Salm et al., 1990 and Salm, 1993) and describes the Coulomb friction μ scaling with the normal stress and the turbulent friction ξ depending on the velocity squared (Christen et al., 2012; Bartelt et al., 2013):

$$S_f = \mu \rho H g \cos(\phi) + \frac{\rho g U^2}{\xi},\tag{4}$$

where ρ is the mass density, g is the gravitational acceleration, ϕ is the slope angle (approximately similar to the internal friction angle of the material), and $H g \cos(\phi)$ is the normal stress on the surface it is over-running. The tangent of the effective internal friction angle of the flow material can be specified for the resistance of the solid phase (the term containing μ) which dominates deceleration behavior when the flow is moving slowly. In contrast, the resistance of the viscous or turbulent fluid phase (the term including ξ) prevails when the flow is moving quickly (Bartelt et al., 2013).

Bartelt et al. (2013) propose a comprehensive method for calibrating the RAMMS debris flow runout model starting with the collection of model input data from a previous event (debris flow volume, discharge hydrograph) and field data which are useful for the calibration of the model (runout pattern, runout distances, flow heights, flow velocities). Secondly, the RAMMS model can be applied by selecting plausible friction parameters (ξ and μ) considering the results of recent model applications and the field data of the study. The final step is to do a comparative analysis of the model outputs and the field data, especially runout pattern data such as runout distance and lateral overflow, front flow travel time and flow heights. The final calibration of the model input parameters can be established using an iterative approach.

The main challenge is to calibrate the runout model using field data varying from event to event. Further corroboration of the simulation results with comprehensive data will increase the confidence in the model results and the parameters used (Christen et al., 2012; Bartelt et al., 2013).

4.2 Debris-flow entrainment model

The entrainment modeling approach outlined in this study is based on field data from the Illgraben catchment in Switzerland. The entrainment model consists of two components, where the potential erosion depth is predicted as a function of channel-bed shear stress, and the vertical erosion rate of channel-bed sediment erosion is constrained by other field observations. Figure 3 illustrates the plausibility of this approach based on the field data from the Illgraben and Spreitgraben catchments.

The erosion data set from Illgraben used as the basis for the model consists of differential elevation models based on pre- and post-event DTMs and an analysis of the depth of net erosion in a cell as a function of the estimate of local
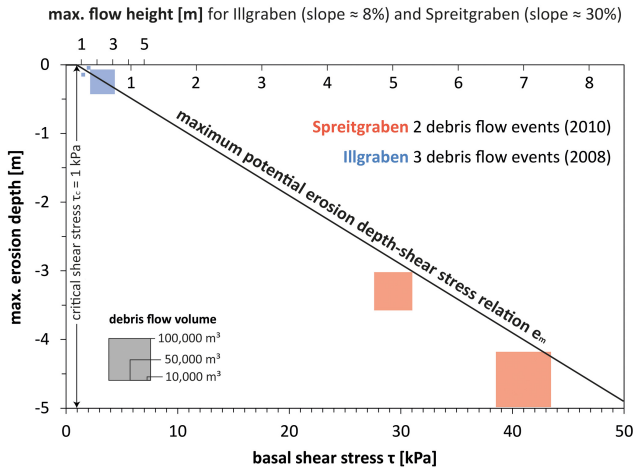
Figure 3. A linear relationship for maximum erosion depth as a function of basal shear stress forms the basis of the model. The size of the boxes is proportional to the estimated event volume at the Illgraben (3 debris-flow events, Berger et al., 2010b) and Spreitgraben (2 events, Geotest, 2010). The upper axis indicates the flow height at the Illgraben (8 % channel slope) with the numbers above the axis, and at the Spreitgraben (30 % slope) with the flow depth values placed below the axis; the corresponding shear stresses (Eq. 5) are plotted at the bottom of the figure.

shear stress at the Illgraben debris-flow catchment (Schürch et al., 2011b). Corresponding flow heights were estimated by Schürch et al. (2011b) using interpolated values between lateral levées of the event. The shear stress τ that is present at a given point at the base of the flow and acting on the channel bed is given by the depth-slope product:

$$\tau = \rho ghS, \tag{5}$$

where ρ is the bulk mass density of the flow, h is flow height, and S is the channel slope. Following the 50 % percentile line describing the distribution of elevation change measured for four debris flow events at the Illgraben (Fig. 3a in Schürch et al., 2011b) we can approximate the average potential erosion depth at the Illgraben as a linear function of shear stress with the proportionality factor $\frac{dz}{d\tau} = 0.1 \, \text{m kPa}^{-1}$.

In the RAMMS model, the erosion algorithm is defined using the maximum potential erosion depth e_m and a specific erosion rate. A linear relationship between maximum shear stress observed and the erosion measured by Schürch et al. (2011b) is used to determine the maximum potential erosion depth (Eq. 6a). It is calculated using a critical shear stress τ_c (= 1 kPa) and an average potential erosion depth $\frac{dz}{d\tau}$ (= −0.1 m kPa^{-1}) as a function of basal shear stress τ.

$$e_m = \begin{cases} 0 & \text{for } \tau < \tau_c \\ \frac{dz}{d\tau}(\tau - \tau_c) & \text{for } \tau \geq \tau_c \end{cases} \tag{6}$$

In addition, an estimated average erosion rate based on values measured at the erosion sensor site during the Illgraben

debris flow event of 1 July 2008 (Berger et al., 2011) is used to define a specific erosion rate $\frac{dz}{dt}$.

$$\frac{dz}{dt} = -0.025 \text{ for } e_t \leq e_m \tag{7}$$

The implemented erosion rate is specifically set to $\frac{dz}{dt} = -0.025 \, \text{ms}^{-1}$ (Eq. 6b) and is active from when the critical shear stress τ_c is exceeded until the actual erosion depth e_t reaches the maximum potential erosion depth e_m (Eq. 6a). The erosion rate prevents the model from entraining all of the potentially available sediment within only one time step. Such rapid entrainment is unrealistic and would result in unrealistically large peak flow discharges. The specific erosion rate can be modified by the user if e.g., local field data are available.

The erosion rates observed at Illgraben (Berger et al., 2011) are consistent with other field observations. From large-scale debris-flow erosion experiments at the US Geological Survey debris flow flume, Reid et al. (2011) reported erosion rates ranging from 0.05 to 0.10 ms^{-1}. Mc-Coy et al. (2012) reported a maximum erosion rate of about 0.14 ms^{-1} within the headwaters of a natural debris flow catchment at Chalk Cliffs, Colorado, USA. The maximum erosion rate measured in the Illgraben (0.25 ms^{-1}) is somewhat larger than reported in the other studies; however, the flows at the Illgraben are also larger in size than in the other studies.

Schürch et al. (2011b) noted that field data showed substantial erosion taking place when a basal shear stress of 3–4 kPa was exceeded. However, a linear fit to the 50 % percentile distribution line on Fig. 3a in Schürch et al. (2011b) results in a critical shear stress τ_c of 1 kPa, below which little erosion was observed. While it would be possible to implement a non-linear fit to the data, this was considered to yield only a small improvement. In addition, larger erosion depths as observed at Spreitgraben (3 to 4 m) could not be represented with the entrainment model because the percentile distribution lines (Fig. 3a in Schürch et al., 2011b) indicate a flattening out of maximum erosion possible to a somehow lower limit of about 1 to 1.5 m of erosion in depth (which may reflect the structure of that data set rather than a real reduction of the slope of the line). Nevertheless, when addressing entrainment modeling of smaller debris flow volumes (some 100 to 1000 m^3) in small channels on lower-slope fans (slope < 10°), it may be necessary or desirable to adjust the critical shear stress threshold for erosion, especially if additional data are available.

The probability of erosion used as the basis for this model does not differentiate between cells where little erosion is expected (e.g., the inside bends of a channel bend) or where significant erosion can be expected (e.g., the outside of channel bends, or the channel thalweg). Additionally, it is likely that local shear stress in the field was different from the values determined by Schürch et al. (2011), because the assumptions

used to estimate the shear stress are simplifications. In real debris flows, the surface of the flow is typically convex up in the lateral direction (so the depth in the shear stress estimate should be somewhat larger than the straight-profile assumption made by Schürch et al. (2011), and the local slope of the debris flow surface at the flow front is perhaps different than the slope-parallel surface assumed here. Additionally, bank collapse, knick-point migration, and other processes may influence the failure and erosion of the channel bed at any given location.

The RAMMS model predicts channel-bed erosion; however, it does not modify the DTM during the simulation. After each model run, it is possible to subtract the predicted erosion depth from the DTM within the user interface of the RAMMS model, thereby permitting the simulation of complicated multi-event scenarios on e.g., the development of topography.

As a model run progresses, the potential erosion depth (as a function of shear stress) is used to set the maximum erosion depth for each grid point in the model, and the sediment in the channel bed is entrained at the specified rate until the potential erosion depth is reached. If the shear stress during an event again exceeds the critical value, then the maximum potential erosion depth (referenced to the bed surface before the simulation) is updated and the channel bed can continue to erode. The model only describes vertical incision and does not consider lateral bank failure as the channel is deepened. Hence, secondary processes such as bank collapse and the resulting deposition of sediment in the channel are not computed within the model.

Instead, the user can specify polygons where the maximum erosion depth in each polygon can be set to a constant value to allow for simulation of flow directly over open bedrock or engineering structures as well as over channel beds covered by sediments at a known depth. Finally, the coefficients in the model (critical shear stress τ_c, potential erosion depth per basal shear stress $\frac{dz}{d\tau}$, erosion rate $\frac{dz}{dt}$) can be adjusted if necessary or if better data become available.

4.3 Entrainment model consistency check at Illgraben, Switzerland

The debris flow event of the 1 July 2008 at Illgraben was chosen to test whether the implemented erosion model (Fig. 3, Eq. 6) based on data mostly collected on the upper fan (Fig. 1d) also functions as expected at the lower fan between check dam 27 and 29 (Fig. 1c). The default model values (Eq. 6) describing the erosion behavior are compared to the observations at check dam 29 as well as to the erosion ranges at the erosion sensor site (Berger et al., 2011).

The total event volume of the debris flow on 1 July 2008 was estimated to be $V \approx 58\,000\,\text{m}^3$. The event lasted about 1 h including several secondary surges. Flow parameters measured at the debris flow observation station on check dam 29 are summarized in Table 2.

To verify that the entrainment model performs in a reasonable manner when implemented in RAMMS, the model was applied to the reach where erosion rates were measured by Berger et al. (2011) (Fig. 1c). The model was started using an input hydrograph (often used term to define flow depth or discharge through time) implemented just above check dam 27 (Fig. 1c). The hydrograph data measured at check dam 29 (about 465 m downstream) were used for calibration in which the friction coefficients μ and ξ (Eq. 4) were systematically adjusted until both the travel time and flow depth are similar to the observed values. The best-fit parameters were found to be $\mu = 0.05$ and $\xi = 1200\,\text{m}\,\text{s}^{-2}$, and the predicted erosion rates are realistic (Table 2).

After calibration of the friction coefficients – which has to be done when using the Voellmy friction relation in every case, even without entrainment – it is clear that the model is capable of re-producing the erosion values observed at the Illgraben channel. This is not surprising, given that the entrainment model was derived from field data at the Illgraben; however, the relation to define the maximum depth of erosion (Eq. 6) was derived from about 1500 m upstream of the main observation site, where the flow velocity can only be roughly constrained. This suggests that the generalization of the entrainment model to define the maximum erosion depth as a function of shear stress may be reasonable, although Berger et al. (2011) argued that pressure fluctuations in the flow, which may be a function of shear stress, could be a physically more realistic way to describe the erosion process. However more work needs to be done to develop an entrainment model based on pressure fluctuations (Deubelbeiss and McArdell, 2012). This topic is beyond the scope of this paper.

5 Entrainment model application results at Spreitgraben, Switzerland

5.1 Entrainment model application setup

The main purpose of the entrainment model application at Spreitgraben is to evaluate how the model performs under these very different boundary conditions such as topography (e.g., steeper channel slope) and flow conditions (larger flow heights, discharges and flow volumes). The 2010 debris flow season was chosen for the modeling because the best quality data at the Spreitgraben are available for this year (Fig. 2b, Table 1). Overall, five debris flow events were documented in 2010 (Geotest, 2010). The three smallest events – each estimated to be $\approx 10\,000\,\text{m}^3$ (Table 1) – were observed to behave more like a debris flood typically characterized by constant flow heights ($\approx 0.5\,\text{m}$) over 30 to 60 min (Geotest, 2010). These three small events did not exhibit steep debris flow fronts and they did not cause significant erosion in the channel. They are therefore neglected herein.

Only the two relatively large debris flow events of 23 July 2010 ($\approx 90\,000\,\text{m}^3$) and 12 August 2010 ($\approx 130\,000\,\text{m}^3$)

Table 2. Best-fit friction coefficients for the RAMMS debris-flow model (Voellmy friction relation, Eq. 4) with entrainment (Eq. 6) at the Illgraben for the 1 July 2008 debris flow (Berger et al., 2011).

	Input Parameters			Results				
	ξ^a (m s^{-2})	μ^b ()	ρ^c (kg m^{-1})	t_t^d (s)	Q_p^e (m^3 s^{-1})	h_{max}^f (m)	v_{max}^g (m^2 s^{-1})	e_r^h (m)
observed	–	–	2000	88	≈ 90	2.35	5.5	0.05–0.30
modeled	1200	0.05	2000	95	85–100	2.2–2.4	5.1–5.8	0.04–0.28

[a] Dry-Coulomb friction μ. [b] Viscous-turbulent friction ξ. [c] Bulk density ρ. [d] Travel time t_t (s) between check dam 27 and 29. [e] Peak discharge Q_p (m^3 s^{-1}). [f] Maximum flow height h_{max} (m) at check dam 29. [g] Maximum flow velocity v_{max} (m^2 s^{-1}) at the erosion sensor site (Berger et al., 2011). [h] Net erosion range e_r (m) at the erosion sensor site (Berger et al., 2011).

were considered. These debris flows caused considerable primary erosion of several meters each (Fig. 3) while leading to secondary erosion processes such as bank collapses (Fig. 8). Comparing the annual debris flow volume of 2010 considering runoff and all deposits in the Aare river between influence of the Spreitgraben and the downstream village of Innertkirchen ($\approx 290\,000$ m^3) with the total erosion volume measured ($\approx 180\,000$ m^3) we calculated, based on the differential elevation data analysis within the bins (Table 1; Fig. 2c), that the total debris flow volume at the lower firn boundary is $V \approx 110\,000$ m^3. This result is consistent with estimates by Geotest (2012) based on sediment input from the rock avalanche, erosion underneath the firn deposits and sediment contribution from lateral channels. The debris flow initiation area was mostly covered by the firn deposits and hence it is difficult to assess (Geotest, 2012). Therefore the estimated annual debris flow volume for 2010 at the lower firn boundary (1.310 m a.s.l.) is chosen as the starting point for the modeling.

The annual debris flow volume is then distributed between the two debris flow events (Table 3) proportional to their total event volumes estimated by Geotest (2012) (Table 1). The two discharge hydrographs required as model input are derived addressing typical debris flow discharge behavior as observed at Spreitgraben (Geotest, 2010) and Illgraben (Berger et al., 2011) using a simplified four-point hydrograph (Table 3) and a correlation between debris flow volume V and peak discharge Q_p proposed by Rickenmann et al. (1999):

$$Q_p = 0.1 \times V^{5/6}. \tag{8}$$

The entrainment model applications are performed using the RAMMS debris flow runout modeling software (version 1.5.01) in which the entrainment model was implemented. The Voellmy friction parameters were varied systematically as $\xi = 200, 500, 1000, 2000$ and $\mu = 0.10, 0.20, 0.25, 0.30, 0.35, 0.40$ in order to investigate the sensitivity of the model results and to find the best overall fit to the field data. The first event (23 July 2010, Table 3) was modeled on the digital elevation model available (April 2010). An updated elevation
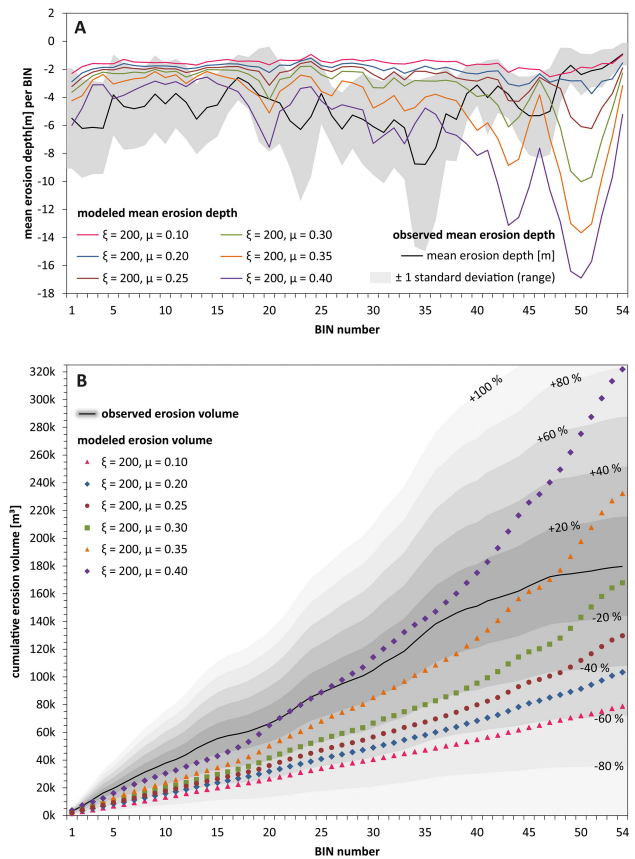

Figure 4. (a) Range of modeled compared to observed mean erosion depths for the two events of 2010 (Table 3). **(b)** Modeled cumulative erosion volumes compared to observed cumulative erosion volumes using the bin-based systematic analysis. The gray shaded areas depict the ranges of percental volume difference compared with the observed erosion volume.

model for the second debris flow (10 August 2010, Table 3) modeling was created based on the erosion modeled for each parameter combination in the first model run (23 July 2010, Table 3) to account for the bed level changes caused by the first debris flow. Finally, the modeled erosion values of both separate model runs were summarized to get the total mod-

Table 3. The two largest debris flow events from 2010 are described by a two-surge input hydrograph used for the runout erosion model testing. Peak discharge Q_p (bold) is derived from debris flow event volumes V (bold) based on Eq. (7).

debris flow event	RAMMS hydrograph point	time t (s) after front arrival	discharge Q_t (m^3 s^{-1}) at time t	volume V_t (m^3) at time t
07/23/2010	1	0	0	0
	2	5	**755**	1888
	3	30	465	17 138
	4	150	0	**45 038**
08/12/2010	1	0	0	0
	2	5	**1025**	2562
	3	30	685	23 937
	4	150	0	**65 037**
Total 2010				**110 075**

eled erosion depths (Figs. 4a and 7), the cumulative erosion volumes (Fig. 4b) and the erosion pattern (Figs. 4 and 7) for the events of 2010.

5.2 Entrainment model application results

The most realistic model result incorporating entrainment modeling was found when the model was calibrated using $\xi = 200$ and $\mu = 0.20$ resulting in a front travel time ≈ 2 min and 30 s between upper fan and gallery of the main road. Because the parameters $\xi = 500$, 1000 and 2000 resulted in front travel times clearly shorter than 2 to 4 min (as estimated in the field, Geotest 2010) while leading at the same time to almost no erosion (~ -0.5 m along the entire channel reach), they were not considered any further in the model sensitivity analysis.

The modeled mean erosion depth per bin using $\mu = 0.20$ and $\mu = 0.25$ generally underestimate observed mean erosion depths along almost the entire channel reach. Despite depicting constant underestimation, simulations with $\mu = 0.10$ interestingly result in accurate mean erosion estimates just above the gallery (bins 48 to 54). The coefficient $\mu = 0.20$ shows no clear consistency with observed values. When choosing $\mu = 0.25$, the model also describes realistic erosion behavior, yet the absolute values are still about 1 standard deviation less than the observed mean erosion values (bins 1 to 38, Fig. 2) covering most of the Spreitgraben channel (Fig. 4a). Modeled mean erosion values per bin using $\mu = 0.30$, $\mu = 0.35$ and $\mu = 0.40$ are mostly located within ± 1 standard deviation of the observed data – excluding two locations where scouring can be identified around bins 43 resp. 50 (Fig. 4a).

Using $\mu = 0.30$, we persistently underestimate erosion by approximately 1 standard deviation (Fig. 4a). Within some short channel reaches (bins 17 to 20 and 38 to 43), the entrainment modeling using $\mu = 0.30$ works quite well but overestimates erosion along the smoother channel reach just above the gallery (bins 48 to 54). Simulations using $\mu = 0.35$

result in very similar mean erosion values. This modeling experiment generally shows slightly more erosion and fluctuating values between -2 and -6 m which is mostly within ± 1 standard deviation range of the observed data (Fig. 4a). Finally, the most realistic spatial erosion pattern is obtained using $\mu = 0.40$. The modeled mean erosion values fluctuate around the observed mean incorporating a large channel reach (bins 1 to 38). Mean observed values are rarely precisely reproduced (only for bins 25 to 33). Nevertheless, these simulations ($\mu = 0.40$) result in an accurate prediction of most of the field data modeled.

The modeled cumulative erosion volumes are somewhat underestimated in comparison with the observed cumulative erosion volumes (Fig. 4b). The corresponding result is also apparent in the modeled flow depths. In the case of $\mu = 0.40$, the cumulative erosion volumes are reasonably well predicted along the upper two-thirds of the channel reach (bins 1 to 36). From bins 37 to 54, the cumulative erosion volumes are increasingly overestimated due to the scouring effect resulting in an overestimation of almost $+100\%$ of the observed cumulative erosion volumes ($\approx 322\,000$ m^3). A similar shaped curve is described by $\mu = 0.35$ whereby it first underestimates the cumulative erosion volumes by $\approx 15\,000$ to $20\,000$ m^3 (-40% for bins 1 to 18 down to -20% for bins 19 to 39) – but finally results in an overestimation of about $+30\%$ ($\approx 232\,000$ m^3). Regarding the overall cumulative erosion volume estimation (all bins), the simulation with $\mu = 0.30$ ($\approx 168\,000$ m^3) is closest to the observed cumulative erosion volume ($\approx 180\,000$ m^3). Using $\mu = 0.30$, the entrainment model also works well along the upper to the middle-range channel reach (bins 1 to 39), while a constant underestimation of about -40% has to be noted. Simulations using $\mu = 0.25$, $\mu = 0.20$ and $\mu = 0.10$ result in predicted cumulative volumes clearly too low compared to observed values (overall -30, -40 and -60%, respectively), while their erosion volume allocation behave similarly at the upper- to middle-range channel reach (bins 1 to 39).
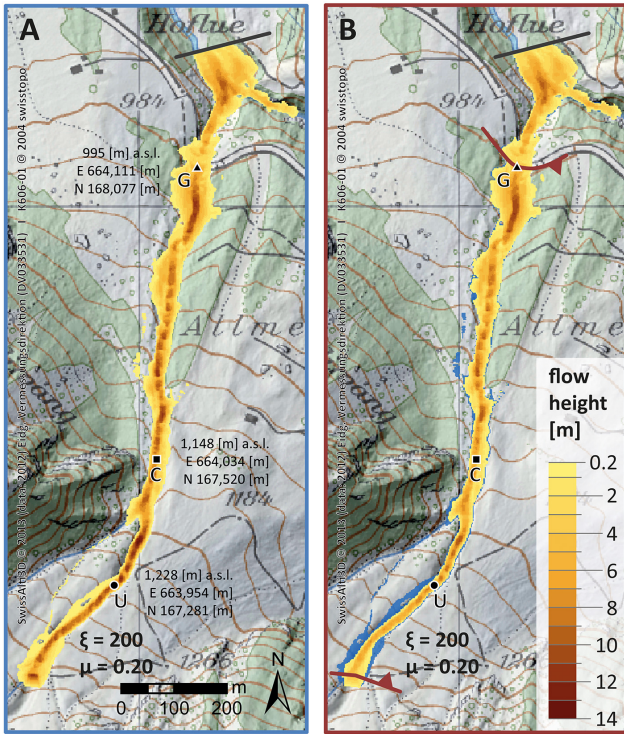
Figure 5. Maximum modeled flow height for the second event on 10 August 2010 (Table 1) using no-erosion modeling **(a)** compared to erosion modeling **(b)**, showing considerable differences in the extent of over-bank flow (**b**: blue area). Locations U (upper fan, Inner Spreitgraben), C (below the confluence) and G (top of the road gallery) are used in Fig. 6.

Figure 6. Comparison of modeled flow height for the second event on 10 August 2010 (Table 1) using no-erosion modeling (blue lines) and erosion modeling (red lines) with distance along the channel. The different modeling locations (U, C, G) are shown in Fig. 5.

Figure 7. Cumulative probability-density plot of modeled vs. observed erosion depths for the two events of 2010 (Table 3) based on a grid resolution of 2 m by 2 m in bins 1 to 54, for a total of 12 621 cells, using the DTMs of April 2010 and August 2010. Erosion is also included and represented on the x axis (< -0.05 m), while no erosion cells and cells with deposition are not included.

Considering all the results related to the choice of friction coefficients, one can conclude that erosion behavior cannot be precisely represented using only one Coulomb friction value for the entire area. This may be related to the complex topography (e.g., slope angles), respectively, that in reality friction angles are not necessarily constant along the channel. While it would be possible to define different friction values for each reach, such fine-tuning does not seem to be warranted in this case because velocity data for the different reaches are not available.

The comparison of modeled and observed erosion depths using the probability density plot offers another method to compare model results. The probability-density analyses of medelled vs. observed erosion depth is based on all the cells (12 621; 2 by 2 m) within bins 1 to 54 (Fig. 7). The probability of occurrence for different erosion depths (discretized into decimeter-scale changes) is calculated for all the parameter combinations considered in the entrainment modeling (Fig. 7).

The model result closest to the field data is the simulation with $\xi = 200$ m^2 s^{-1} and $\mu = 0.30$, although there is a slight trend to under-predict maximum erosion depth and to over-predict the area with lower erosion depths. Part of this
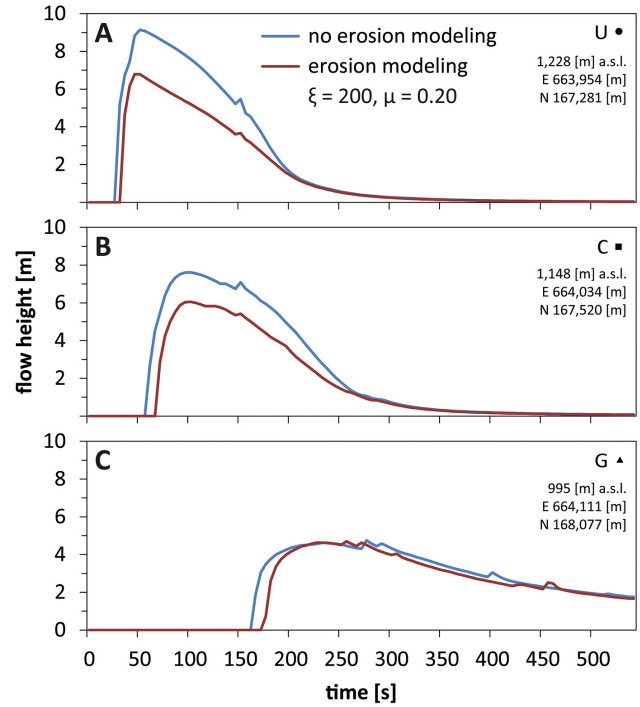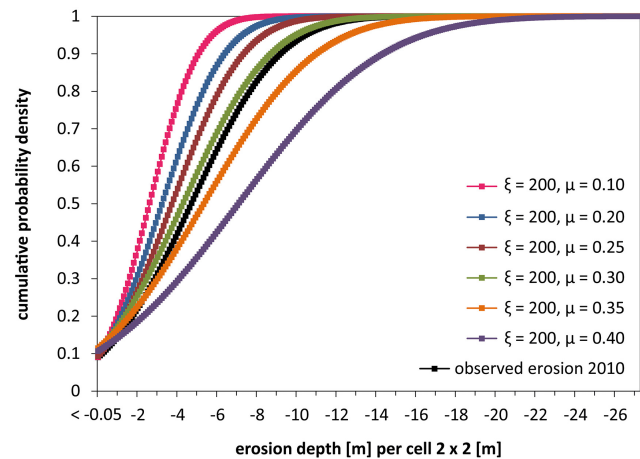
discrepancy can be explained by processes other than debris-flow erosion, such as bank collapse and the re-working of sediment within the channel by smaller flood flows. This result is also somewhat different from the best-fit entrainment
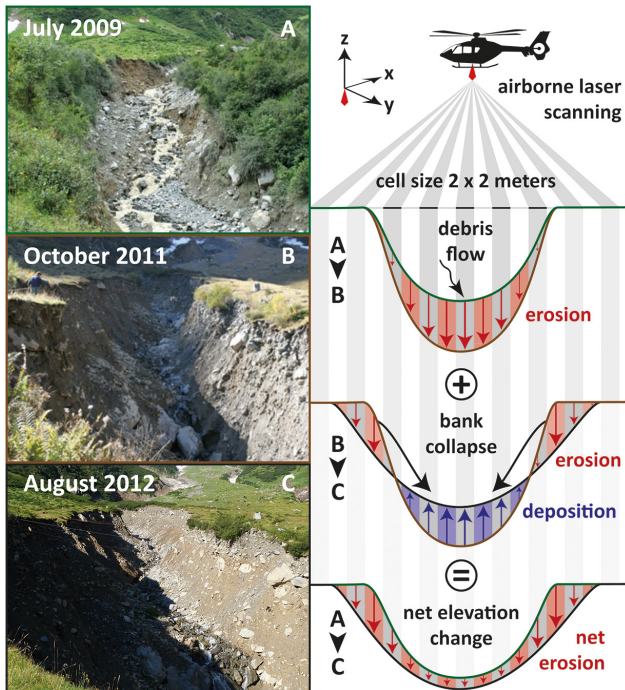
Figure 8. Conceptual model for the evolution of the debris-flow channel, in three stages, at the Spreitgraben during the three active years after the re-activation of the channel following the first large debris flow July 2009 (photos taken by Geotest in 2009 and 2011, by Florian Frank in 2012). Several reiterations showing primary erosion (**a** to **b**) by debris flow degradation and secondary erosion (**b** to **c**) composed of lateral bank collapses result in channel degradation and widening, while the channel bed is often composed of fresh and easily erodible sediment deposits. Shaded columns are indicating observed erosion and deposition volume per cell. Arrows represent the mean erosion and deposition measured.

model results regarding runout pattern and lateral over-flow (Sect. 6.1), where the most realistic result was achieved using $\xi = 200\,\mathrm{m^2\,s^{-1}}$ and $\mu = 0.20$. A more detailed investigation of the best-fit friction coefficients is not possible at this field site due to the imprecision in the observed flow properties (e.g., travel time over the entire reach) which would be necessary for a more precise model calibration.

6 Discussion

6.1 Flow properties and runout patterns

One important aspect of this modeling study was to evaluate how including entrainment affects the runout modeling of debris flows. This includes the influence on flow properties such as the mean front flow velocity and the change in flow height over time which describes the flow hydrograph. The results show that the incorporation of debris-flow entrainment modeling within a runout model can improve the overall prediction of runout.

Using the RAMMS debris flow runout model without entrainment modeling, the most plausible modeled flow properties (front travel time and hydrograph shape) can be achieved using Voellmy friction coefficients of $\xi = 200\,\mathrm{m^2\,s^{-1}}$ and $\mu = 0.20$. This calibration was done applying the standard RAMMS debris flow runout model without entrainment modeling for the largest debris flow event at Spreitgraben (12 August 2010; Geotest, 2010) which had an estimated volume of $130\,000\,\mathrm{m^3}$ (Table 1) with the total volume entering the computational domain at the lower firn boundary (Fig. 2b and c).

The runout entrainment model was implemented using a realistic initial flow volume of about $50\,000\,\mathrm{m^3}$ at the lower firn boundary which produced similar total flow volumes at the gallery (Table 1; location G in Fig. 5) within $\pm 10\,\%$ of the estimated event volume at that location. The resulting maximum flow heights as well as the hydrograph using the entrainment modeling approach are similar to the fixed-bed modeling and consistent with observed peak flow heights of about 5 to 7 m (Figs. 5 and 6c). The comparison of runout modeling with and without entrainment modeling shows several differences in runout patterns (Fig. 5). The runout entrainment modeling improves the modeled runout pattern by reducing most of the lateral overflow obtained in the fixed-bed modeling approach. Such lateral bank overflows were not observed in the field, although, some individual smaller rocks were ejected from the debris flow due to the highly turbulent flow behavior (Geotest, 2010).

A comparison of the flow depth through time (often referred to as the hydrograph) for both runout model types (fixed-bed vs. entrainment) at Spreitgraben also shows substantial differences between the models (Fig. 6). Due to the smaller initial volume and discharge, the entrainment model (Fig. 6, red lines) has corresponding smaller maximum flow heights on the upper fan (Fig. 6a) and below the confluence with the Outer Spreitgraben (Fig. 6b) by about 2 to 2.5 m which results in fewer lateral overbank outbreaks (Fig. 5).

The reduction of the lateral overflow area is noticeable along the upper channel reach (blue area in Fig. 5c). The two main subsequent outbreaks of ~ 100 to $1000\,\mathrm{m^3}$ predicted by the fixed-bed model at approximately 100 m and again at 200 m below location C (both on the orographic left side) are not present in the runout modeling result (Fig. 5b). In this example, the entrainment model provides a clearly more realistic result in comparison with the fixed-bed model.

Observed front travel times are not well constrained for the 2010 Spreitgraben events. Estimates range from 2 to 4 min between the upper channel (location U) and the gallery (location G) (Geotest, 2010). The two different models produce similar overall travel times, e.g., about 2 min 15 s with the fixed-bed model and about 2 min 20 s using the entrainment runout model (Fig. 6a compared to Fig. 6c). The corresponding mean front flow velocity from bin 1 to 54 along the central flow line ($\approx 1340\,\mathrm{m}$ in April 2010) is $\approx 9.9\,\mathrm{m\,s^{-1}}$ for the fixed-bed runout model and $\approx 9.6\,\mathrm{m\,s^{-1}}$ for the en-

trainment runout model. Estimates of flow velocities from oblique video images gave debris flow front velocities of $\approx 8\,\mathrm{ms}^{-1}$ at the flow front and of $\approx 5\,\mathrm{ms}^{-1}$ just after the flow front had passed (Geotest, 2010). The maximum modeled flow velocities on the top of the gallery (location G) were found to be ≈ 5.0–$8.0\,\mathrm{ms}^{-1}$ for the entrainment model and ≈ 4.5–$7.5\,\mathrm{ms}^{-1}$ for the fixed-bed model during and shortly after peak discharge and are within the observed range of $\approx 8.0 \pm 2\,\mathrm{ms}^{-1}$ (Geotest, 2010).

The similar front arrival times of modeled hydrographs indicate that the standard model calibration procedure proposed for the RAMMS debris-flow model without entrainment (Bartelt et al., 2013) might be also appropriate for the entrainment modeling approach. Therefore, we suggest that the basic calibration process can be enhanced by applying the entrainment model while using previously calibrated parameters ξ and μ. Nevertheless, more comparisons of fixed-bed and entrainment model have to be conducted in other catchments to judge the reliability of the suggested enhancement of the model calibration process.

The entrainment modeling investigations presented in this paper emphasizes the requirement for an entrainment model implemented in debris-flow models to improve flow behavior along the channel and inundation patterns on the fan, especially for highly erosive debris flows.

Berger et al. (2011) suggested that entrainment influences the motion of the debris flow because the entrained sediment has to be accelerated from a state of rest up to the speed of the flow; this could be visible in an additional resistance near the flow front. To include entrainment in a debris-flow model, Hussin et al. (2012) predefined one or more erosion layers with a specific thickness which are fully eroded in their model when exceeding a critical shear stress. They noted that the entrainment method used in their erosion model showed high sensitivity to event volume and flow heights in their study at the Faucon catchment in the southern French Alps. Their approach can deliver accurate results and improve the runout patterns results when back-calculating a previous well-documented debris-flow event. However, their approach requires pre-determined information about the potential erosion depth (layers) normally not available except for past and well documented events. Therefore, this concept is not directly suitable to assess the amount of entrainment for future debris flow surges as required for hazard assessment. This problem can only be addressed by predefined entrainment rates based on physical concepts or entrainment rates measured in laboratories or in the field. For example, Medina et al. (2008) implemented an entrainment model where the erosion process is activated if the shear stress exceeds the resistance at the channel bed using a static as well as a dynamic approach. The dynamic approach uses momentum-driven entrainment rates where the entrained mass has to be accelerated to the mean flow velocity.

The entrainment model proposed in this study characterizes the erosion process based on the idea that the maximum depth of erosion (Fig. 3, Eq. 6). is a function of basal shear stress (Eq. 4). Hence, the entrainment model does not require pre-defined maximum erosion depths. Noticeable differences in modeled runout patterns are expected to emerge for larger flow heights, larger volumes, steeper (and less distinctive) channel slopes and larger bulk densities (e.g., characteristic of granular debris flows). By constraining the rate of erosion by field observations of erosion rates, we account for the suggestion that natural debris flows show rather different erosion behavior than down-scaled laboratory experiments (Iverson and Denlinger, 2001; Rickenmann et al., 2003; Reid et al., 2011; McCoy et al. 2013). The empirical approach using potential erosion depths as well as erosion rates observed in the field offers the opportunity to estimate the expected amount of debris-flow entrainment and its effects on hydrograph propagation and runout. Nevertheless, further model tests are necessary to further corroborate the accuracy of this approach.

6.2 Probability occurrence of erosion depths

In general, the Spreitgraben channel was relatively stable prior to the very large debris flow in 2009, although there is a chronology of small debris flows in the past. The debris flow process itself primarily causes vertical deepening of the channel bed (Fig. 8a). This results in an increase in the height and overall steepness of the channel banks, which failed to lower, more stable friction angles (Fig. 8b), with the sediment stored in the channel. The net result is that the channel becomes wider, and with net removal of sediment in the channel bed (e.g., due to debris flow or flood erosion), there is a net lowering of the channel (Fig. 8c).

Therefore, we suggest that the slightly higher probability of the observed upper-range erosion values of more than $-10\,\mathrm{m}$ (see Fig. 4a and Fig. 7) are due to the collapse of lateral banks. In situ observations of the two larger Spreitgraben debris flow events 2010 showed that such secondary erosion processes were regularly occurring within hours up to several days after the debris flow events. Hence, they are related to but not directly caused by the larger debris flows (Geotest, 2010). Highest erosion values were observed especially along the former banks of the channel on the upper fan where the erosion values measured for 2010 are even larger than along the central flow line (Fig. 2c; bins 1 to 15). This indicates that the bank collapses are causing at least some portion of the higher probability of large net erosion depths observed (more than $-10\,\mathrm{m}$). Because there is a lack of knowledge about the exact timing, locations and volumes of these lateral collapses in 2010 (this study started in July 2012), it was impossible to conduct a temporal or quantitative analyses of the collapses. Thus, the lateral bank collapses (Figs. 2c and 8) and their influence on the net erosion values observed (Fig. 7) remain unquantified.

The discussion above raises the possibility that a geomorphic threshold was exceeded which caused the destabiliza-

tion of the channel on the debris fan and resulted in the debris fan becoming a source of sediment for large debris flows instead of being a depositional environment. The mechanism is that the channel bed was first strongly eroded by the first large debris flow. This deepened the channel and resulted in a condition where the over-steepened banks partially collapsed (Fig. 8), greatly increasing the amount of sediment available for transport. Subsequent debris flows could then entrain this sediment, thereby increasing their size and causing more channel-bed erosion. This may have also resulted in considerably higher erosion rates at the Spreitgraben than predicted by the erosion model (Fig. 3, Eq. 6b) based on the erosion rates measured at Illgraben (Berger et al., 2011). Although such positive feedback mechanisms are plausible, they are difficult to explicitly test. Regarding the initial channel "re-activation" event in 2009, our estimate is that the shear stress must have exceeded ~ 5 kPa during the first flow, which is consistent with field observations in 2012 and 2013 where smaller debris-floods with estimated maximum shear stress values of ≈ 4–5 kPa did not cause significant channel-bed erosion.

7   Conclusions

The development, implementation and application of the debris-flow entrainment model (Sects. 4 and 5) highlights the importance of entrainment for runout modeling. The entrainment model is based on the relation between calculated basal shear stress and the net erosion (Schürch et al., 2011b) as well as an erosion rate (Berger et al., 2011) which were both measured at the Illgraben channel. The entrainment model was evaluated at the Spreitgraben channel and, without additional calibration beyond that necessary for the standard fixed-bed model, the model delivers results which are in agreement with field data regarding channel-outbreak patterns and the depth of erosion. Other parameters such as pressure fluctuations due to particles in the flow impacting the bed could provide a more realistic physical basis to describe erosional behavior. However, the model presented herein may be useful until more physically accurate algorithms become available.

The comparison of two RAMMS runout results, either ignoring or including entrainment (Sect. 6) illustrates that including entrainment can substantially improve the prediction of spatial runout patterns (Fig. 5, Sect. 6.1) as well as flow propagation (Fig. 6). Nevertheless, more sensitivity testing of the erosion model has to be conducted to assess the usefulness of the model to other geometric settings and field conditions (e.g., channel slope and event volume). We suggest that inconsistencies between the observed and modeled net elevation change can partly be explained due to erosion originating from different processes (Fig. 8) such as lateral bank collapse and due to increased erodibility of correspondent sediment deposits. We conclude that including sediment erosion and the resulting volume growth due to entrainment in debris-flow runout modeling can considerably improve the accuracy of model results.

References

Badoux, A., Graf, C., Rhyner, J., Kuntner, R., and McArdell, B. W.: A debris flow alarm system for the Alpine Illgraben catchment: design and performance, Nat. Hazards, 49, 517–539, 2009.

Bartelt, P., Salm, B., and Gruber, U.: Calculating dense-snow avalanche runout using a Voellmy-fluid model with active/passive longitudinal straining, J. Glaciol., 45, 242–254, 1999.

Bartelt, P., Buehler, Y., Christen, M., Deubelbeiss, Y., Graf, C., and McArdell, B. W.: RAMMS – rapid mass movement simulation, A modeling system for debris flows in research and practice, user manual v1.5, debris flow, manuscript update: 31 January 2013, WSL Institute for Snow and Avalanche Research SLF, available at: http://ramms.slf.ch/ramms/downloads/RAMMS_DBF_Manual.pdf (last access: 27 February 2015), 2013.

Beguería, S., Van Asch, Th. W. J., Malet, J.-P., and Gröndahl, S.: A GIS-based numerical model for simulating the kinematics of mud and debris flows over complex terrain, Nat. Hazards Earth Syst. Sci., 9, 1897–1909, doi:10.5194/nhess-9-1897-2009, 2009.

Bennett, G. L., Molnar, P., Eisenbeiss, H., and McArdell, B. W.: Erosional power in the Swiss Alps: Characterizing slope failure at the head of the Illgraben, Earth Surf. Proc. Land., 37, 1627–1640, 2012.

Bennett, G. L., Molnar, P., McArdell, B. W., Schlunegger, F., and Burlando, P.: Patterns and controls of sediment production and transfer in the Illgraben, Switzerland, Geomorphology, 188, 68–82, 2013.

Bennett, G. L., Molnar, P., McArdell, B. W., and Burlando, P.: A probabilistic sediment cascade model of sediment transfer in the Illgraben, Water Resour. Res., 50, 1225–1244, 2014.

Berger, C., McArdell, B. W., Fritschi, B., and Schlunegger, F.: A novel method for measuring the timing of bed erosion during debris flows and floods, Water Resour. Res., 46, W02502, doi:10.1029/2009WR007993, 2010a.

Berger, C., McArdell, B. W., and Schlunegger, F.: Sediment transfer patterns at the Illgraben catchment, Switzerland: Implications for the time scales of debris flow activities, Geomorphology, 125, 421–432, 2010b.

Berger, C., McArdell, B. W., and Schlunegger, F.: Direct measurement of channel erosion by debris flows, Illgraben, Switzerland, J. Geophys. Res., 116, F01002, doi:10.1029/2010JF001722, 2011.

Christen, M., Kowalski, J., and Bartelt, P.: RAMMS: Numerical simulation of dense snow avalanches in three-dimensional terrain, Cold Reg. Sci. Technol., 63, 1–14, 2010.

Christen, M., Bühler, Y., Bartelt, P., Leine, R., Glover, J., Schweizer, A., Graf, C., McArdell, B. W., Gerber, W., Deubelbeiss, Y., Feistl, T., and Volkwein, A.: Integral hazard management using a unified software environment: numerical simulation tool "RAMMS" for gravitational natural hazards, edited by: Koboltschnig, G., Hübl, J., Braun, J., 12th Congress INTER-PRAEVENT, 23–26 April 2012 Grenoble, France, Proceedings, Vol. 1, Klagenfurt, International Research Society INTER-PRAEVENT, 77–86, 2012.

Crosta, G. B., Imposimato, S., and Roddeman, D. G.: Numerical modelling of large landslides stability and runout, Nat. Hazards Earth Syst. Sci., 3, 523–538, doi:10.5194/nhess-3-523-2003, 2003.

D'Ambrosio, D., Di Gregorio, S., and Iovine, G.: Simulating debris flows through a hexagonal cellular automata model: SCID-DICA S3-hex, Nat. Hazards Earth Syst. Sci., 3, 545–559, doi:10.5194/nhess-3-545-2003, 2003.

Deubelbeiss, Y. and McArdell, B. W.: Dynamic modelling of debris-flow erosion and deposition with application to the USGS debris flow flume experiments, Geophys. Res. Abstr. 14, EGU2012-7906, 2012.

Gabus, J. H., Weidmann, M., Bugnon, P.-C., Burri, M., Sartori, M., and Marthaler, M.: Geological map of Sierre, LK 1278, sheet 111, scale 1:25,000, in Geological Atlas of Switzerland, Swiss Geol. Surv., Bern, Switzerland, 2008.

Geotest AG, Zollikofen BE/CH: Several reports about the debris flow events from 2009 to 2011 at the Spreitgraben catchment, Switzerland, 2010–2012.

Graf, C., Deubelbeiss, Y., Bühler, Y., Meier, L., McArdell, B., Christen, M., and Bartelt, P.,: Gefahrenkartierung Mattertal: Grundlagenbeschaffung und numerische Modellierung von Murgängen, in: Mattertal – ein Tal in Bewegung, Herausgeber: Graf, C., Publikation zur Jahrestagung der Schweizerischen Geomorphologischen Gesellschaft, 29 June yo 1 July 2011, St. Niklaus, Birmensdorf, Eidg. Forschungsanstalt WSL, 85-1-12, 2013.

Huggel, C., Clague, J. J., and Korup, O.: Is climate change responsible for changing landslide activity in high mountains? Earth Surf. Proc. Land., 37, 77–79, 2011.

Hungr, O. and McDougall, S.: Two numerical models for landslide dynamic analysis, Comput. Geosci., 5, 978–992, 2009.

Hungr, O., McDougall, S., and Bovis, M.: Entrainment of material by debris flows, in: Debris-flow hazards and related phenomena, edited by: Jakob , M. and Hungr, O., Springer, Berlin, New York, 135–158, doi:10.1007/b138657, 2005.

Hürlimann, M., Rickenmann, D., and Graf, C.: Field and monitoring data of debris-flow events in the Swiss Alps, Can. Geotech. J., 40, 161–175, 2003.

Hussin, H. Y., Quan Luna, B., van Westen, C. J., Christen, M., Malet, J.-P., and van Asch, Th. W. J.: Parameterization of a numerical 2-D debris flow model with entrainment: a case study of the Faucon catchment, Southern French Alps, Nat. Hazards Earth Syst. Sci., 12, 3075–3090, doi:10.5194/nhess-12-3075-2012, 2012.

Iverson, R. M.: The physics of debris flows, Rev. Geophys., 35, 245–296, doi:10.1029/97RG00426, 1997.

Iverson, R. M. and Denlinger, R. P.:Flow of variably fluidized granular masses across three-dimensional terrain: 1. Coulomb mixture theory, J. Geophys. Res., 106, 537–552, 2001.

Iverson, R. M., Reid, M. E., Logan, M., LaHusen, R. G., Godt, J. W., and Griswold, J. G.: Positive feedback and momentum growth during debris-flow entrainment of wet bed sediment, Nat. Geosci., 4, 116–121, doi:10.1038/NGEO1040, 2011.

Jakob, M. and Hungr, O.: Debris-flow hazards and related phenomena, Springer, Berlin, New York, 170 pp., 2005.

Kienholz, H., Frick, E., and Gertsch, E.: Assessment tools for mountain torrents: SEDEX© and bed load assessment matrix. Congress INTERPRAEVENT 2010 – Grenoble/France, Conference proceedings, available at: www.interpraevent.at (last access: 27 February 2015), 2010.

Kober, F., Hippe, K., Salcher, B., Ivy-Ochs, S., and Kubik, P. W.: Debris-flow-dependent variation of cosmogenically derived catchment-wide denudation rates, Geology, 40, 935–938, 2012.

Mangeney, A., Bouchut, F., Thomas, N., Vilotte, J. P., and Bristeau, M. O.: Numerical modeling of self-channeling granular flows and of their levee-channel deposits, J. Geophys. Res., 112, F02017, doi:10.1029/2006JF000469, 2007.

McArdell, B. W., Bartelt, P., and Kowalski, J.: Field observations of basal forces and fluid pore pressure in a debris flow, Geophys. Res. Lett., 34, L07406, doi:10.1029/2006GL029183, 2007.

McCoy, S. W., Kean, J. W., Coe, J. A., Staley, D. M., Wasklewicz, T. A., and Tucker, G. E.: Evolution of a natural debris flow: In situ measurements of flow dynamics, video imagery, and terrestrial laser scanning, Geology, 38, 735–738, doi:10.1130/G30928.1, 2010.

McCoy, S. W., Kean, J. W., Coe, J. A., Tucker, G. E., Staley, D. M., and Wasklewicz. T. A.: Sediment entrainment by debris flows: In situ measurements from the headwaters of a steep catchment, J. Geophys. Res., 117, F03016, doi:10.1029/2011JF002278, 2012.

McCoy, S. W., Tucker, G. E., Kean, J. W., and Coe, J. A.: Field measurement of basal forces generated by erosive debris flows, J. Geophys. Res.-Earth, 118, 589–602, doi:10.1002/jgrf.20041, 2013.

Medina, V., Hürlimann, M., and Bateman, A.: Application of FLAT-Model a 2-D finite volume code, to debris flows in the northeastern part of the Iberian Peninsula, Landslides, 5, 127–142, 2008.

Reid, M. E., Iverson, R. M., Logan, M., LaHusen, R. G., Godt, J. W., and Griswold, J. G.: Entrainment of bed sediment by debris flows: results from large-scale experiments. in Fifth International Conference on Debris-flow Hazards Mitigation, Mechanics, Prediction and Assessment, edited by: R. Genevois, Hamilton, D. L., and Prestinizi, A., Casa Editrice Universita La Sapienza, Rome, 367–374, 2011.

Rickenmann, D.: Empirical Relationships for Debris Flows. Swiss Federal Institute for Forest, Snow and Landscape Research, CH-8903 Birmensdorf, Nat. Hazards 19, 47–77, 1999.

Rickenmann, D. and Zimmermann, M.: The 1987 debris flows in Switzerland: documentation and analysis, Geomorphology, 8, 175–189, 1993.

Rickenmann, D., Weber, D., and Stepanov, B.: Erosion by debris flows in field and laboratory experiments, in: Proceedings of the Third International Conference on Debris-Flow Hazard Mitigation: Mechanics, Prediction and Assessment, edited by: Rickenmann, D. and Chen, L. C., 10–12 September, Davos, Switzerland, Milpress, Rotterdam, the Netherlands, 883–894, 2003.

Salm, B.: Flow transition and runout distances of flowing avalanches, Ann. Glaciol., 18, 221–226, 1993.

Salm, B., Burkard, A., and Gubler, H.: Berechnung von Fliesslawinen: eine Anleitung für Praktiker mit Beispielen, Mitteilung 47, Eidg. Institut für Schnee- und Lawinenforschung SLF, Davos, Switzerland, 1990.

Scheuner, T., Schwab, S., and McArdell, B. W.: Application of a two-dimensional numerical model in risk and hazard assessment in Switzerland, in 5th DFHM, Padua, Italy, 2011.

Schürch, P., Densmore, A. L., Rosser, N. J., Lim, M., and McArdell, B. W.: Detection of surface change in complex topography using terrestrial laser scanning: application to the Illgraben debris-flow channel, Earth Surf. Proc. Land., 36, 1847–1859, 2011a.

Schürch, P., Densmore, A. L., Rosser, N. J., and McArdell, B. W.: Dynamic controls on erosion and deposition on debris-flow fans, Geology, 39, 827–830, 2011b.

Sovilla, B., Burlando, P., and Bartelt, P.: Field experiments and numerical modelling of mass entrainment in snow avalanches, J. Geophys. Res., 111, F03007, doi:10.1029/2005JF000391, 2006.

Tobler, D., Kull, I., Jacquemart, M., and Haehlen, N.: Hazard Management in a Debris Flow Affected Area: Case Study from Spreitgraben, Switzerland, Landslide Science for a Safer Geoenvironment, 3, 25–30, doi:10.1007/978-3-319-04996-0_5, 2014.